Chapter 6

Sulphur deposition experiment

Optical fibres can be used for indirect monitoring of SF_6 in an SF_6 discharge. During an SF_6 discharge, dissociation processes cause free sulphur to be deposited on the wall of the discharge chamber (Bunganaen, 1993). The technique applied here is based on the measurement of the free sulphur deposited on an optical fibre placed in a discharge chamber. A method has been developed for measuring the amount of deposited sulphur and it is described in this chapter.

6.1. Experimental Arrangement

The first experiment for investigating sulphur deposition from an SF_6 discharge was carried out using a white light source. The experimental arrangement is depicted in figure 6.1. The light source is an ORIEL Q housing lamp with a 250 W, 24 V quartz tungsten halogen bulb. Lenses made of BK7 glass are used to collimate and launch the light from the lamp into the fibre. The fibre passes through a glow discharge chamber, as shown in figure 6.1. The sealing of the chamber, where the fibre goes in and out of the chamber, is made with Torr-Seal® adhesive (manufactured by Varian). The output end of the fibre is mounted to the input of a SPEX MINIMATE-2 (SPEX Industries Inc., USA) 1/4 m monochromator with a 1200 lines/mm grating and 0.25 mm slits. The detector attached at the output of the monochromator is an EMI 9558QB photomultiplier. The monochromator is equipped with a scanning controller. Both the controller and the photomultiplier are connected to a National Instrument acquisition board as part of a Macintosh computer. The spectrum from the output

of the fibre is scanned and stored in the computer for further analysis. The output signal from the photomultiplier is amplified with a photodiode current amplifier and the output signal is set to between 0 and 5 V which is the range of the acquisition card.

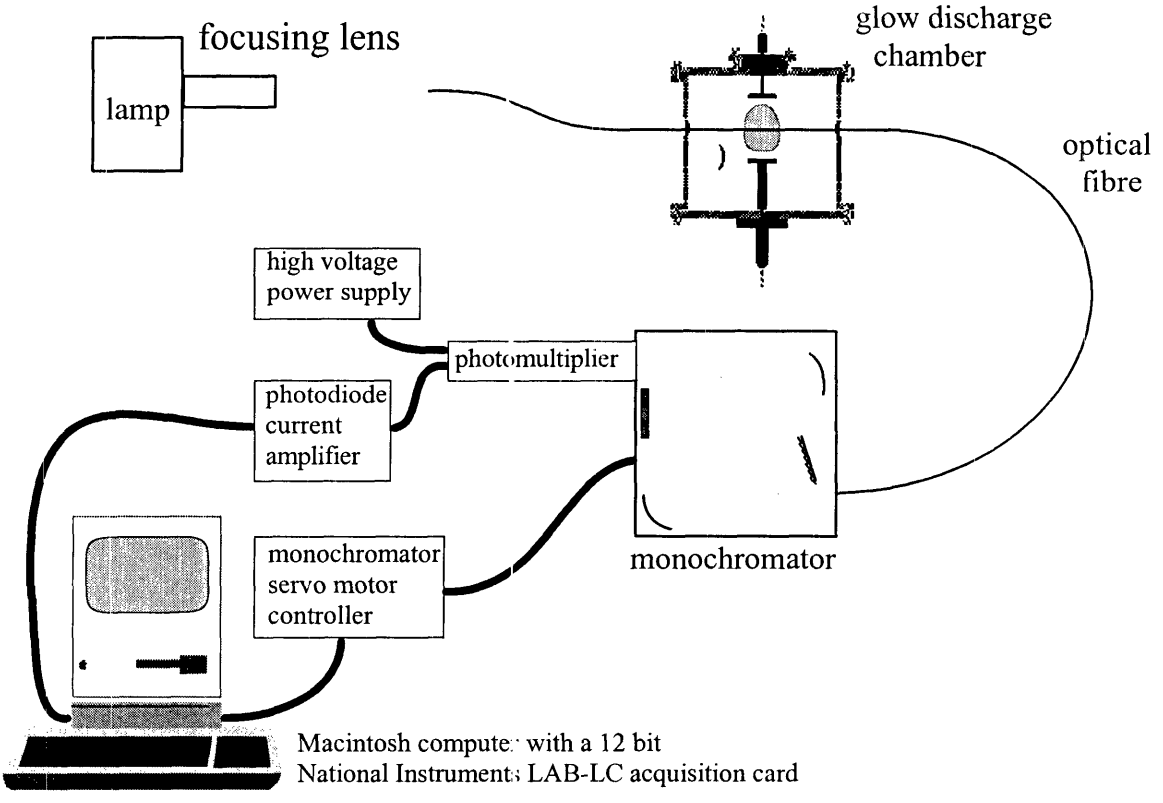

Figure 6.1. Experimental arrangement for the measurement of sulphur deposition on an uncladed PCS optical fibre, using a white light source.

6.1.1. Optical Fibre Preparation

PCS (polymer-clad silica) 600N PUV fibre from Ceram Optec is used for this experiment. It was chosen because of handling convenience: the siloxane cladding is easy to remove. For stripping a 2.5 cm length, it is possible to use a finger nail. A scalpel is used for removing the jacket. The use of a scalpel is not recommended for removing the cladding because the fibre core, made of silica, may be scratched. Apart from changing the optical characteristics, scratching reduces the mechanical strength of the fibre, which is already

greatly reduced by removing the cladding and jacket. The core is made of silica, and with a thickness of 0.6 mm, it is very brittle in the absence of the cladding and jacket. Since for unclad regions longer than 5 cm the fibre needs to be handled very carefully, it was preferable to strip the cladding chemically using Lumer optical fibre stripper "S". The main components of this stripper are methylene chloride and sulphuric acid. For the first experiment with white light, 15 cm of the fibre was unclad and placed inside the chamber. Both cladding and jacket were removed with the Lumer optical fibre stripper "S". The chamber was filled with SF_6 to 0.96 Torr and a glow discharge was maintained for 7 hours. Spectra were taken every 30 minutes. At the same time as a spectrum was taken, a sample of the gas mixture from the chamber was analysed using the mass spectrometer.

6.2. Absorption measurements using a white light source

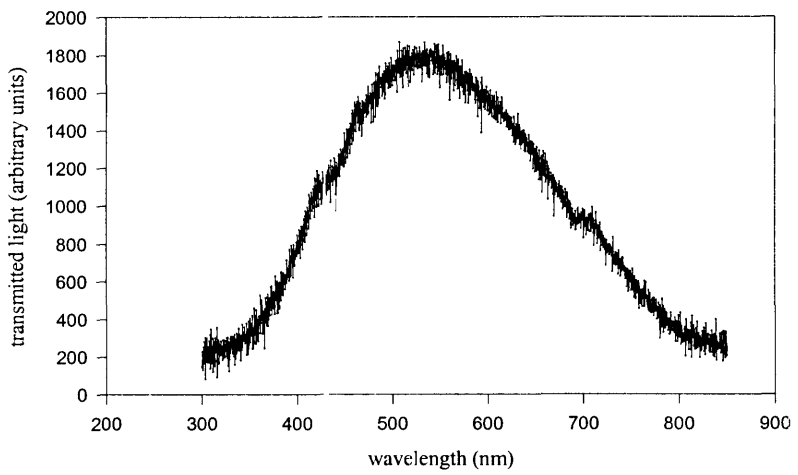

Figure 6.2. The spectrum of the light transmitted through the fibre

6.2.1. Absorption Spectra

The transmitted light spectrum taken before the discharge started is shown in figure 6.2. The spectrum obtained after filtering with a fast Fourier transform and raised

cosine filter is shown in figure 6.3. The same filter is applied to the signals recorded during the glow discharge. Three samples of transmission spectra are shown in figure 6.4: the top curve is at the beginning, before the discharge starts; the middle curve after 2 hours of discharge and the bottom one, after 3 hours and 10 minutes. Absorption spectra are derived from the relationship

$$absorption\ spectrum = 1 - \frac{transmission\ spectrum}{top\ curve\ in\ figure\ 6.4} \tag{6.1}$$

Two absorption curves are shown in figure 6.5, together with details of discharge times and total charge transferred.

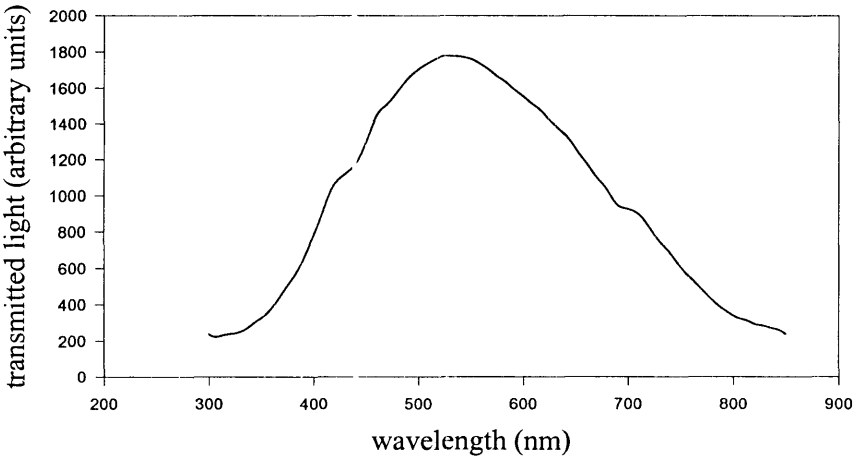

Figure 6.3. The same spectrum as in figure 6.2 but filtered from noise.

6.3. Absorption measurements using a He-Ne laser

From figure 6.5 it is seen that after 2 hours there is a relatively higher absorption in the blue than over the remainder of the spectrum, but later, when a thicker layer of sulphur builds on the optical fibre, the higher absorption in the blue region is less pronounced. In later experiments, the white light was replaced with a 10 mW polarised He-Ne

laser (figure 6.6). A microscope objective (magnification = 60, numerical aperture = 0.85) was used to launch the laser light into the fibre. After a few experiments it was found that the best sensitivity was obtained when the system was aligned as follows. The single-mode optical fibre coupler that holds the fibre was first adjusted until the maximum reading at the output was obtained; at that time the output of the fibre was a bright spot. Measurements were made, however, with the fibre tilted until a distinctive doughnut pattern was observed at the output; this time the output power was about 20% less than the maximum reading. This alignment arrangement maximises the interaction between the laser light transmitted through the fibre and the deposited sulphur. A silicon photodiode was used as detector and the signal was recorded on a chart recorder after being amplified. A 3 cm length of cladding was removed from the PCS 600N PUV fibre. The fibre was placed in the glow discharge chamber with the unclad region close to the chamber wall. The glow discharge was maintained for 7 hours at 10 mA current, which gave a total charge transfer of 252 C. The intensity of the light transmitted through the fibre was recorded on a chart recorder. The results of the absorption measurements are discussed in section 6.5.

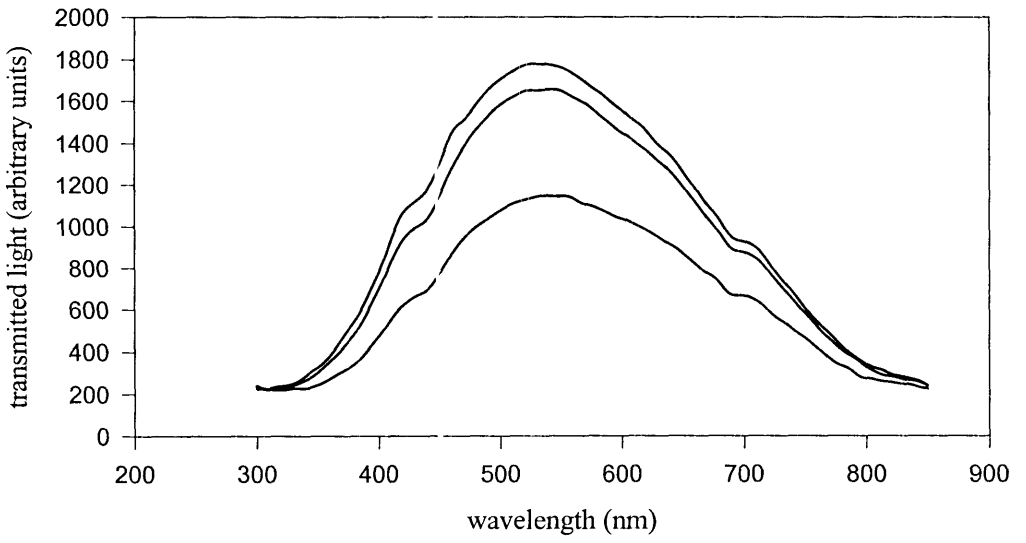

Figure 6.4. The top curve is the starting one. The middle curve was obtained after 2 hours of the glow discharge, and the bottom curve after 3 hours and 10 minutes of discharge.

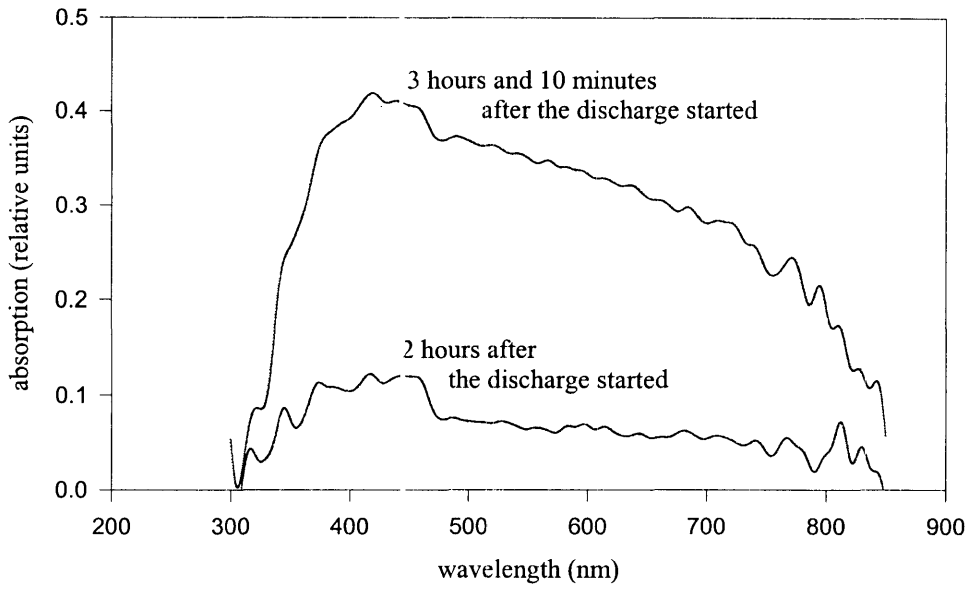

Figure 6.5. Absorption spectra after 2 hours (72 C) and 3 hours and 10 minutes (114 C).

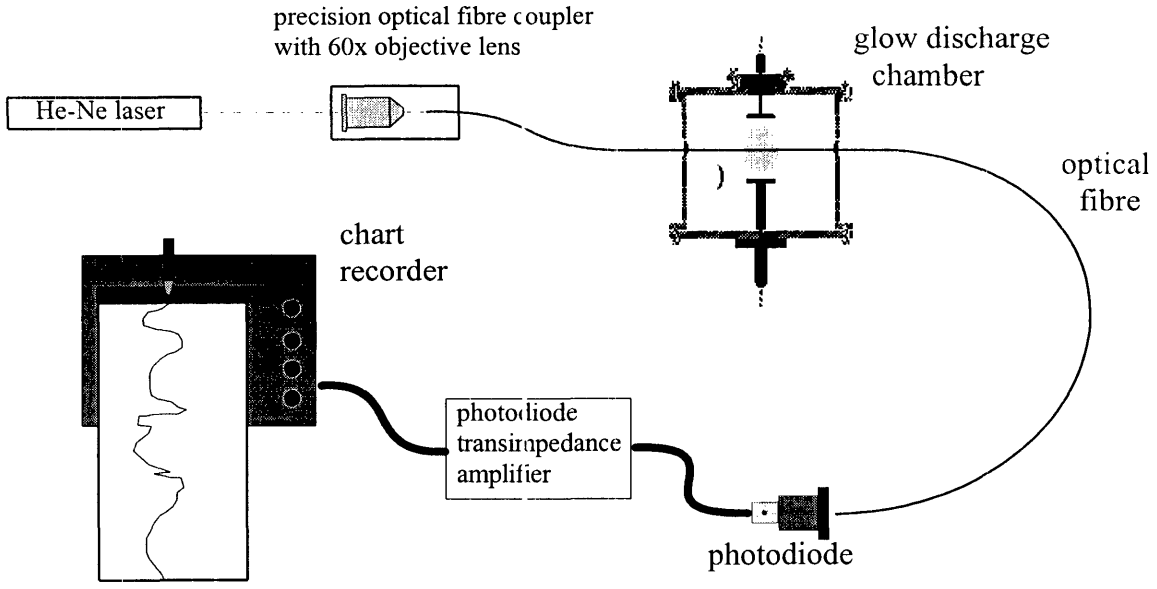

Figure 6.6. Experimental arrangement for the measurement of sulphur deposition on an uncladed PCS optical fibre, using a helium-neon laser.

6.4. Electron microscope probe analysis

Electron microscope probe analysis (with X-rays) reveals that the deposit on the fibre is sulphur. A piece of the 15 cm length of unclad PCS 600N PUV fibre, which was placed in the glow discharge chamber for 7 hours, was used for probe analysis with the electron microscope. The analysis requires the fibre to be coated with carbon. A piece of the fibre close to the chamber wall, complete with sulphur deposit, was analysed in the electron microscope. Figure 6.7 (b) shows the result of the analysis in which only sulphur, silicon, oxygen and carbon were detected. Carbon comes from the coating, while silicon and oxygen are components of silica (SiO_2). Figure 6.7 (a) was obtained for reference using an unused piece of PCS fibre core.

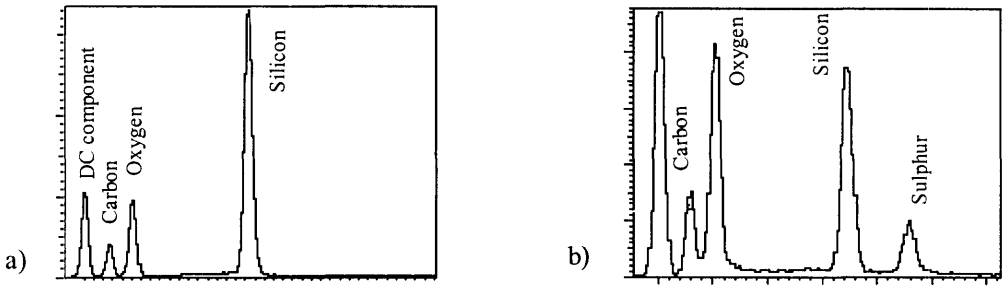

Figure 6.7. Electron microscope probe data: (a) fibre core (silica) in absence of a discharge (b) fibre core (silica) following a 7-hour glow discharge. Quantitative comparisons of pulse amplitudes cannot be made because of the nature of the electron-probe technique.

A part of the unclad fibre that was between the electrodes also was examined. Probe analysis shows that there are other materials in the coating of this sample, such as iron and chromium. They are released from the electrodes. The coating is cracked and uneven due to the high temperature, up to 1000 °C, in the discharge centre (Ogle and Woolsey, 1987). Electron micrographs of the fibre placed near the discharge wall and in the discharge centre, are shown in figures 6.8 (a) and (b), respectively.

From figure 6.8 (b) it can be seen that the thickness of deposited sulphur for a fibre from the centre of the discharge varies widely, since the high temperature of the

discharge causes cracks and flaking of the sulphur deposits. This suggests that measurements of sulphur deposition on a centrally positioned fibre are unlikely to be useful. The following studies are concentrated therefore on measurements made using fibres positioned near the wall of the chamber. Even in this region a few cracks do occur in the sulphur coating on the fibre. These can be seen in figure 6.9 which has a magnification of 30 times that of figure 6.8 (a).

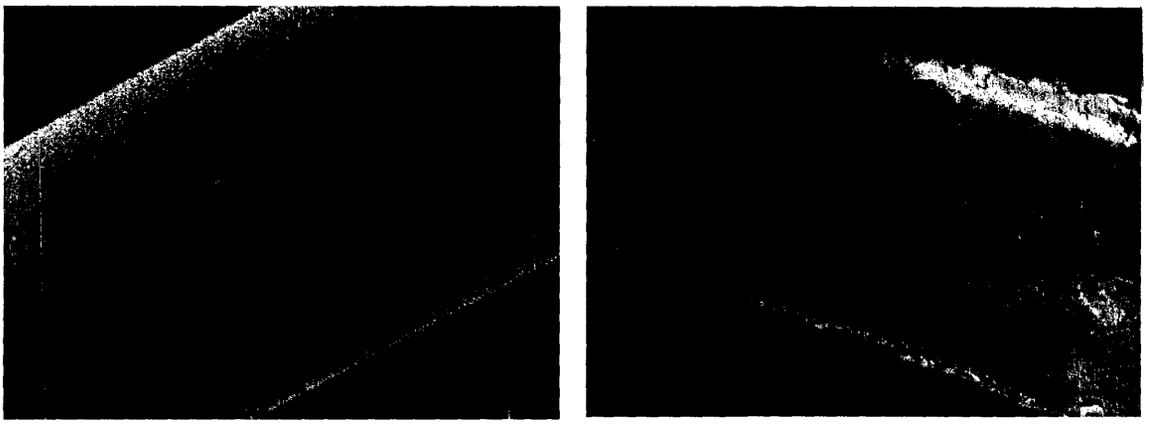

a) b)

Figure 6.8. a) An SEM (scanning electron microscope) picture of the fibre placed near the wall of the glow discharge chamber. The width of the picture is 880 μm and the SEM accelerating voltage is 20 kV. b) An SEM picture of the fibre in the centre of the glow discharge. The picture width is 880 μm, and the accelerating voltage is 20 kV.

Figure 6.9. An SEM picture of sulphur deposited on a fibre placed near the wall of the discharge chamber. The picture width is 33 μm, and the SEM accelerating voltage is 20 kV.

The layer of sulphur deposited on the 600 μm - diameter fibre is very thin, as can be observed in figure 6.10 (a). In order to estimate the thickness of the deposition, a wall fibre was exposed to four consecutive glow discharges, each of 7 hours duration and current 10 mA. Prior to each of these discharges, the chamber was evacuated and filled again with fresh SF_6. After 7 hours of glow discharge almost all sulphur-containing gases were dissociated. The sulphur derived from the initial SF_6 remained as powder on the surfaces of the chamber and the optical fibre. It seems reasonable to assume that after four discharges with initially undissociated SF_6, the thickness of deposited sulphur is around 4 times that following a single discharge.

a) b)

Figure 6.10. The cross section of the fibre with deposited sulphur: a) after 7 hours of discharge (the picture width is 880 μm, SEM accelerating voltage 20 kV); (b) after exposure to four separate glow discharges, each of seven-hours duration (the picture width is 13.2 μm, SEM accelerating voltage 20 kV)

An estimate of the thickness of sulphur coating on a fibre can be obtained from a figure such as 6.10 (b). For this particular electron microscope picture an estimate of 2.4 μm was made. This suggests that the sulphur deposition following one discharge is around 600 nm.

6.5. Experimental results and discussion

The curve shown in figure 6.11 was obtained when the He-Ne laser was used in the transmission experiment. In this figure there is a distinctive step that occurs as a sulphur layer builds up on the optical fibre. The intensity of the output light starts to fall after 75 C of charge has been transferred through the glow discharge (point 1). The mass spectrometer analysis shows that at that time there was approximately 25% of the initial concentration of SF_6 remaining in the chamber. This leads to the conclusion that the sulphur deposited on the chamber wall and fibre is produced from product gases rather than directly from SF_6. The concentration of SF_6 left in the chamber following the transfer of 140 C (point 2) is around 10% of the initial concentration.

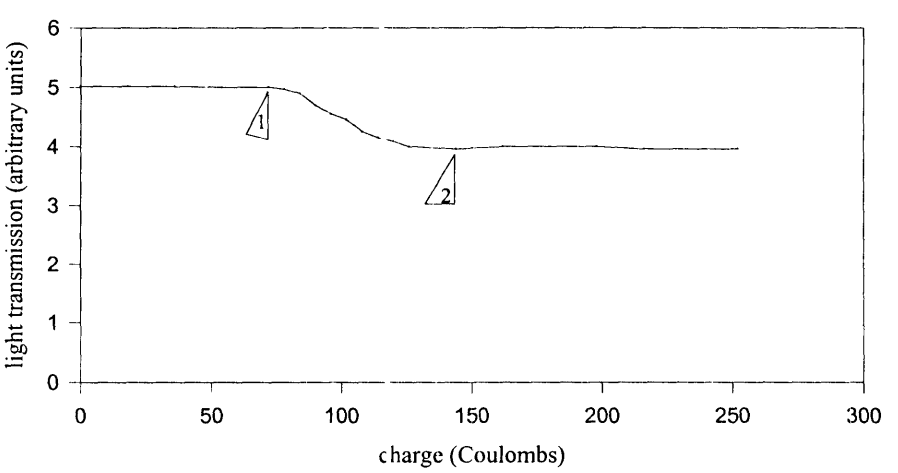

Figure 6.11. The output from the optical fibre when sulphur was being deposited on it.

The curve of figure 6.11 was obtained each time the fibre was cleaned and a further SF_6 discharge generated using a fresh filling of SF_6. When a further discharge was run without removing sulphur from the fibre there was no further change in the light transmission. Also, it was observed that light escapes along the length of the unclad fibre following

deposition of sulphur. This is the scattered light that is coupled into the sulphur layer by refraction or via the evanescent field.

There are several mechanisms which may account for the observation of output signal attenuation and emission along the length of the unclad fibre.

Sulphur is a biaxial material and its refractive indices along three axes are 1.95, 2.043 and 2.24 (Gray, 1972). These values are higher than the refractive index of the core of the fibre and so total internal reflection should not occur. However, the refractive index of the deposited sulphur layer may be lower than these measured values because the pressure in the chamber is high (1 Torr) and the deposited sulphur has a sponge-like structure as shown in figure 6.10. (b). If the refractive index of the sulphur layer is higher than the refractive index of the core, the light will escape mainly by refraction and point 2 in figure 6.11 will be reached when the exposed core becomes fully covered by sulphur.

There is also the possibility of the existence of a thin gap between the core and the sulphur layer. In this case frustrated total reflection will occur and the light will propagate in the same direction through the sulphur as it would in the absence of a gap, but with a lower intensity.

Another possible mechanism involves penetration of the evanescent field of the light in the core into the sulphur layer. As shown below, the penetration depth is expected to be around 100 nm. In order to estimate how deep the evanescent wave spreads around the fibre, it is assumed that the refractive indices of the core (fused silica) and the cladding (polymer) are 1.457 (Malitson, 1965) and 1.400 (Gowar, 1984, page 86), respectively. Because the light is launched into the fibre at an angle, as described in section 6.3, in order to maximise the evanescent field, and because the core is very thick (0.6 mm diameter), the propagation can be treated as propagation in a planar waveguide. In that case the critical angle for the glass/polymer boundary is 73° 55'. In the unclad region the critical angle for the glass/vacuum boundary is 43° 20'. When the light reaches the unclad region only the rays between 73° 55' and 90° are present. The other rays have been refracted into the cladding before they reach the unclad region. Using the wavelength of the He - Ne laser, 633 nm, and 73° 55' for the angle of incidence, the equation for the penetration depth (see appendix 4)

$$d_p = \frac{\lambda_0}{2\pi n_1 \sqrt{\sin^2\alpha - \left(\frac{n_2}{n_1}\right)^2}} \tag{6.2}$$

gives 103 nm for the penetration depth (d_p), where λ_0 is the vacuum wavelength. α is the angle of incidence to the normal of the interface (core - gas in this case) and n_1, n_2 are the refractive indices of the core and surrounding SF_6 gas, respectively (n_1 = 1.457 and n_2 = 1). d_p is the distance over which the evanescent field amplitude falls to e^{-1} of its value at the boundary when the core is in a vacuum or gas. This is in acceptable agreement with the measured thickness of the deposited sulphur: 600 nm (see section 6.4). The derivation of equation 6.2 is presented in Appendix 4.

6.6. Conclusion

The result suggests that this optical fibre method of sulphur deposition measurement could be appropriate for the detection of SF_6 dissociation in high-voltage SF_6 switchgear. Conditions in the present study are very different to those encountered in a practical gas-insulated high voltage device. In this experiment the glow discharge chamber was filled with 0.96 Torr of SF_6. Sulphur deposition on the optical fibre was detectable when 75% of the initial SF_6 concentration in a glow discharge at 0.96 Torr was dissociated: this corresponds to 0.72 Torr (0.00095 atm) partial pressure. The pressure in a high-voltage switching device on the other hand, can be as high as 10 atm. A pressure of 0.72 Torr is only 0.0095% of 10 atm. This suggests that the optical fibre deposition method could provide a very sensitive method of measuring the degradation of SF_6 in a high-voltage switch.

The sensitivity of the sensor could be tailored to suit the particular switch by

(i) choosing the position of the fibre within the high-voltage system,

(ii) placing a shield in an appropriate position around the fibre,

(iii) choosing the length of the unclad fibre section,

(iv) choosing an appropriate fibre diameter,

(v) launching the light in a particular way.

The ultimate test of the applicability of the optical fibre technique, including its long-term reliability, is, of course, its performance in a practical SF_6 - insulated system.

Chapter 7

Experiment on CO_2 laser light absorption

The measurement of SF_6 concentration, using CO_2 - laser absorption of the evanescent wave in a silver halide optical fibre, is based on the 948 cm^{-1} absorption line of SF_6. The SF_6 absorption spectrum from 2 μm to 25 μm is shown in figure 7.1. It was recorded by Lagemann and Jones (1951). As seen in figure 7.1, SF_6 has strong absorption peaks at around 10.7 μm and 16.3 μm. Chapados and Birnbaum (1988) measured the lower wavelength to be at 948 cm^{-1} (10.5485 μm). An analysis with better resolution shows that the peak is closer to 10.55 μm (Rabinowitz *et al.*, 1969). The wavelength of the peak varies for different investigators. According to the most recent measurement (Messica *et al.*, 1994), it is 10.562 μm. The value with highest precision comes from Bobin *et al.* (1987): 947.9763358 cm^{-1} (10.548786528 μm). In fact, the SF_6 line spectrum has over 1000 lines/cm^{-1} in the region of 10.6 μm (Kildal and Deutsch 1976; Hinkley 1970). However, the 10.55 μm line is the strongest and is close to the CO_2 laser line P(16) at 10.5513950296 μm (Maki *et al.*, 1994). These features of CO_2 laser light and the SF_6 absorption spectrum have been employed for measuring SF_6 concentrations using a grating CO_2 laser or a diode laser tuned to 10.55 μm (Sun and Wittaker 1993; Shimizu 1969). But the absorption is so high that this method is suitable only for low pressures. For example, no signal can be detected when light from a 2 W CO_2 laser is passed through a 10 cm cell containing 2 Torr pressure of SF_6 at room temperature. Increasing the power of the laser is not a solution because it may dissociate SF_6 molecules if raised too high; even a few watts of laser power can cause dissociation when focussed inside the cell. This saturation is not a problem, however, when the CO_2 - laser radiation is transmitted through an optical fibre and absorption occurs as a result of an evanescent-field interaction with the SF_6.

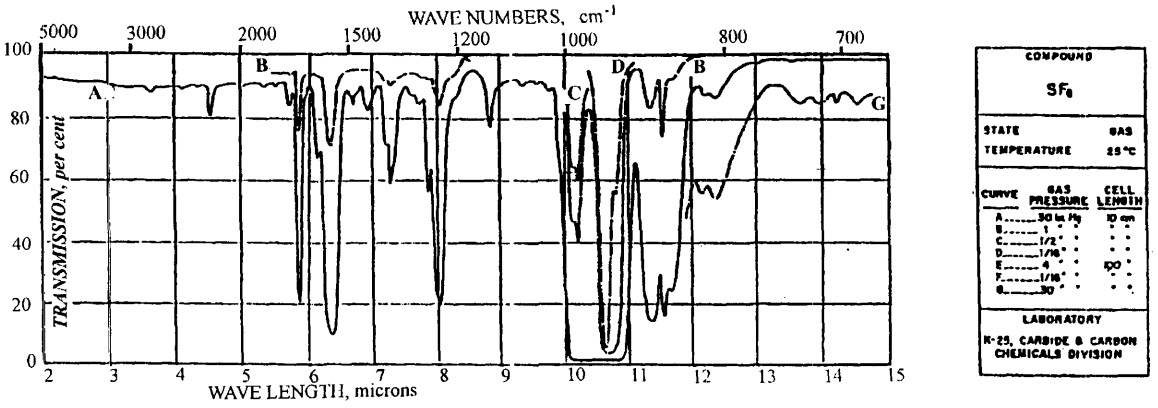

Figure 7.1. The SF_6 infrared absorption spectrum (from Lagemann and Jones, 1951)

As mentioned earlier, the evanescent-field absorption by SF_6 at the P(16) CO_2 laser line, using an optical fibre, is more appropriate for higher pressures. This is demonstrated in recent work where a silver halide optical fibre and a tunable laser diode were used to measure concentrations of SF_6 (Messica *et al.*, 1994). As shown in figure 7.2 the peak at 10.562 μm is distinctive and is very close to the CO_2 laser P(16) line. Silica fibres, as used for communications, are not suitable because they are not transparent beyond 4 μm. Nor are fluoride-containing fibres, for the same reason. For the mid-infrared region which includes CO_2 laser light, silver halide fibres (Simhony *et al.*, 1986), thallium halide fibres (Grigorjeva *et al.*, 1996) and chalcogenide glass fibres (Sanghera *et al.*, 1994) are suitable. Some metal fluoride optical fibres are transparent at 10.6 μm, but they are not as good as silver halide fibres because of their higher absorption at this wavelength. However, the possibility of using these fibres for measuring SF_6 concentration should be investigated when they become commercially available.

7.1. Experimental arrangement

The experimental arrangement for measuring the amount of SF_6 in the corona discharge chamber is shown in figure 7.3. The laser used was a SYNRAD 48G-2-28w CO_2

grating laser. A circular aperture of 1.5 mm diameter was placed in front of the laser output. A ZnSe beam splitter divided the beam in the ratio 2:1, with two thirds of the power entering the monochromator. One third was incident on the ZnSe biconvex lens, which collimated the light, so that it was launched into the fibre at an angle of 45° to the fibre axis. The fibre passed through a 25 cm long cylinder connected to the glow discharge chamber as described in chapter 3. The glow discharge chamber was connected to the corona chamber via a 1.5 m long tube as described in chapter 3. A pyrodetector (Murata IRA-E600S0) detected the infrared light at the output of the fibre. The signal from the pyrodetector was amplified, extracted with the lock-in amplifier ORIEL model 70707, and recorded on a chart recorder. The reference signal for the lock-in amplifier was supplied by the digital signal generator that modulates the laser. The signal from a pyrodetector ORIEL model 70841 attached to the monochromator was amplified with an ORIEL amplifier/readout model 70701, extracted with the lock-in amplifier PAR model 124, and recorded on a chart recorder.

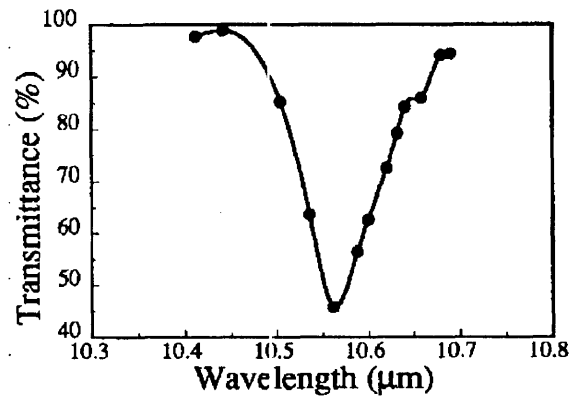

Figure 7.2. The SF_6 absorption spectrum around 10.6 μm (Messica *et al.*, 1994). The peak in the curve is at 10.562 μm.

The signal from this pyrodetector is proportional to the power of the laser and is used to compensate any fluctuation in the laser power. The pressure and temperature in the corona chamber were monitored. These values are used to calculate the pressure of the same

density at 25 °C and the percentage of SF_6 in the corona discharge chamber. During a corona discharge the pressure rises as dissociation occurs, because more molecules are produced. Dissociation of SF_6 molecules in the discharge environment can lead to several events. These include sulphur deposition on the chamber wall, reactions which produce sulphur oxyfluorides, and production of SiF_4 as a result of reaction between fluorine and glass windows. The net effect of all such events is to produce a significant number of additional molecules and a consequent rise in the total gas pressure in the corona chamber.

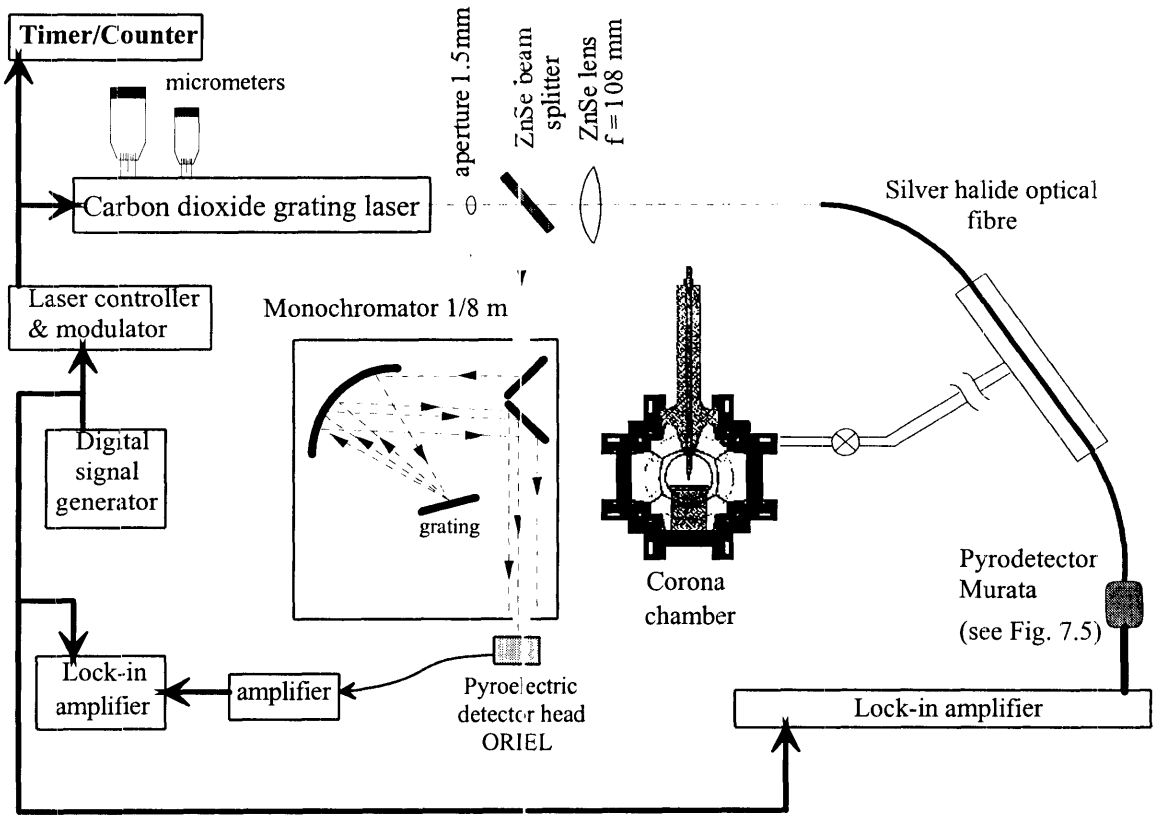

Figure 7.3. Experimental arrangement for measuring evanescent-field absorption during an SF_6 corona discharge.

7.1.1. The grating laser SYNRAD 48G-2-28w

The grating laser SYNRAD 48G-2-28w requires water cooling. Water flow needs to be constant within ±3% and at least 3.6 litres per minute. The recommended temperature of the

water is 20 °C and it should not vary by more than ±0.1 °C, although ±0.01 °C is preferred. These cooling conditions are provided by an attached cooler NESLAB RTL-211D. Two micrometers on top of the laser are used to select the lasing line. The large one is used to change the angle of the grating. It selects the laser spectral line. The smaller one is used to adjust the length of the optical cavity. Using this micrometer it is also possible to change the wavelength within a few tens of megahertz around the spectral line. This also happens if the temperature of the cooling water is not constant. If the temperature is not constant the laser stays within the defined line, but drifts a few megahertz on either side. At maximum output optical power, the grating and cavity length are set for the required spectral line. TEM mode changes were observed during laser warm-up prior to experimental run. During the experiment, mode changes were not observed.

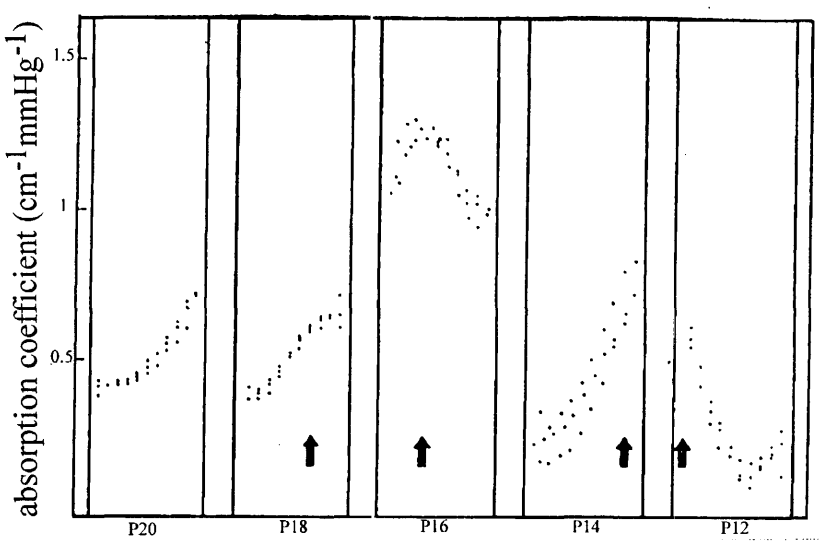

Figure 7.4. The absorption coefficient of SF_6 around the CO_2 laser spectral lines (P12, P14, P16, P18 and P20). The width of the x-axis for one spectral line is estimated to be between 40 and 50 MHz (from Shimizu , 1969). The arrows show the centres of the spectral lines.
The centres of these lines are (Maki *et al.*, 1994):
P12 - 10.5131216772 μm
P14 - 10.5320883339 μm
P16 - 10.5513950296 μm
P18 - 10.5710454539 μm
P20 - 10.5910434604 μm

7.1.2. Source-fibre coupling

The coupling of laser light into the fibre is not very efficient but this is not a problem. Indeed, the power after the ZnSe lens must be maintained below 60 mW. The reason for this is that, in the same way that the SF_6 absorbs light via the evanescent field, other materials in contact with the fibre also absorb light. Torr-Seal®, a two-component adhesive for vacuum applications, is used to seal the fibre at ends of the cylinder, and where the Torr-Seal® contacts the fibre it absorbs CO_2 laser light and thus heats up. This heat is transferred to the fibre and softens it at those points. At higher power the fibre melts at the point closer to the input.

The limit of 60 mW was set for a launching angle of the beam into the optical fibre of 19°. When the launching angle increases this limit increases, because more power is reflected from the input end of the fibre. Equation 7.1 can be used to show that the intensity of the light reflected from the fibre input face increases (when the light is coupled into the fibre) when the incident angle with respect to the fibre axis is increased. Also, it will be used to estimate the power absorbed by the Torr-Seal®. The reflection coefficient from a flat dielectric surface, defined as the ratio of the reflected and incident electric field wave amplitudes, is given by (Collin, 1991) :

$$R = \frac{Z_T - Z_I}{Z_T + Z_I} \tag{7.1}$$

where

Z_I is the wave impedance of the incident medium,

Z_T is the wave impedance of the refracted medium,

$Z = \sqrt{\frac{\mu}{\varepsilon}} = \frac{Z_0}{n}$, where μ is the magnetic permeability and for most optical components it is equal to the magnetic permeability of vacuum (nonmagnetic substances), ε is the dielectric constant, Z_0 is the impedance of vacuum and n is the refractive index. There are two sets of equations for R, Z_T and Z_I. One is for s-polarisation and one for p-polarisation. However, only s-polarisation will be considered here. In figure 7.3, the fibre lies in the plane of the page

and the laser beam is polarised in the direction normal to the page. Consequently, the laser beam enters the fibre as an s-polarised beam and propagates through the fibre as mainly TE mode. This provides better sensitivity in an FEFA sensor than TM mode coupling (see the calculation in section 5.2.3.1). For s-polarisation,

$$Z_S = \frac{E}{H\cos\theta} \tag{7.2}$$

which finally provides an expression for the electric field reflection coefficient of the s-polarised light

$$R_S = \frac{n_I\cos\theta_I - n_T\cos\theta_T}{n_I\cos\theta_I + n_T\cos\theta_T}. \tag{7.3}$$

This equation is one of Fresnel's equations (Lorrain and Corson, 1970).
R_S^2 gives the value of the reflected power.

When the incident angle is 19° the reflected power is 14% of the incident power. When 60 mW of laser power is transmitted through the lens, 51.6 mW is coupled into the fibre. When the pyrodetector was replaced with a power meter at the output, the power recorded was 14 mW. Hence, 37.6 mW was absorbed by the two Torr-Seal® joints.

Having recorded this limit to the power of the laser, the power was set at a substantially lower level to ensure that no over-heating of the sealing points occurred. During the absorption measurement the output power from the laser was 38 mW, and following the 1.5 mm aperture, the power was 6.3 mW. Two-thirds of this power was reflected from the beamsplitter into the monochromator, and 2.1 mW was directed onto the ZnSe lens: this lens has an antireflective coating, and focal length of 4.25" (107.95 mm). The lens was used to launch the light into the fibre. The launching angle was 45° and 22.4% of the input power was reflected at the input face of the fibre. The remaining 1.63 mW was coupled into the fibre and around 0.445 mW was detected at the output.

The laser power was maintained at a constant level using the following procedure. The power of the laser is controlled by a modulator, with a duty cycle of 5 kHz

pulses. Initially a power meter was placed in front of the laser output. The average laser power of 38 mW was obtained using 5.8 μs wide pulses. This width was measured with a digital counter (see figure 7.3). Then the power meter was removed and the pulse width, as monitored by the digital counter, was maintained at around 5.8 μs. For all measurements; at different incident angles and during the corona discharge, no power meter was used. This method of monitoring the laser power was preferred to the use of a beam splitter to direct some fraction of the laser beam to a power meter, since the introduction of another optical component adds noise to the system.

7.1.3. Pyrodetectors

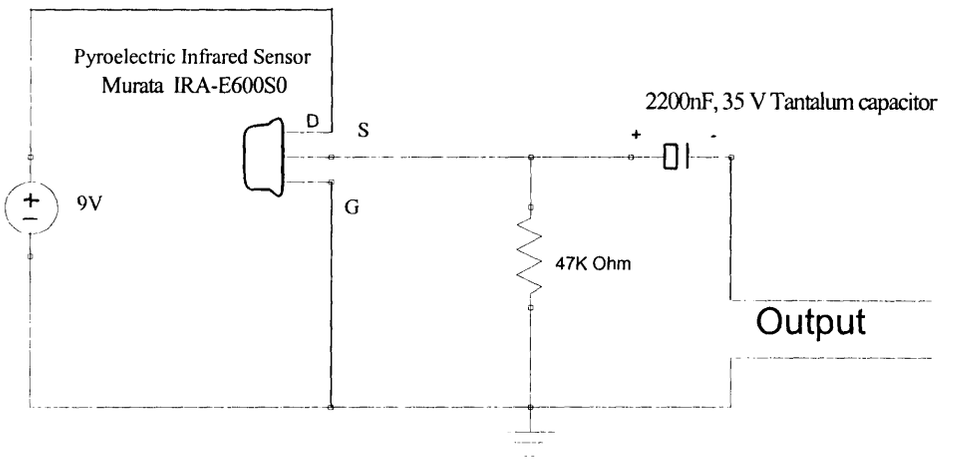

Figure 7.5. The electric circuit for the mid-infrared light detector used for the measuring the light at the output of the fibre.

After adjustment of the laser power level, the power meter at the output of the fibre was replaced by the Murata IRA-E600S0 pyrodetector which is used for all further measurements of the output light from the fibre because the precision and the resolution of the power meter is much lower than those of the pyrodetector. This detector incorporates a piezoelectric crystal that generates electrical charge when pressure is applied to it. A temperature change produces a similar effect. The power of the light from the fibre raises the temperature of the crystal. A constant heat input to the detector does not generate a signal, for

which reason the light beam must be chopped. Here, the laser beam was modulated with a 17 Hz, 50% duty cycle square-wave signal from a digital signal generator. The piezocrystal is encapsulated in a transistor-like case together with a FET transistor. A silicon window in the case transmits light from 1 μm to 20 μm. To obtain a signal from the detector, the circuit shown in figure 7.5 was assembled.

The monochromator used in the experiment (see figure 7.3) was equipped with an ORIEL pyrodetector model 70841 with a *KBr* window, which operates on the same principle as the Murata unit.

7.1.4. The ORIEL 1/8 m monochromator

The 1/8 m monochromator from ORIEL with grating 77302 (75 lines/mm, 7 μm blaze wavelength) has a resolution of 8 nm (20 GHz) with a 0.05 mm slit. This resolution is good enough to indicate when the laser is on the defined spectral line, but it does not show up any drift around the spectral line due to thermal instability, and this instability can be as large as ± 100 MHz. SF_6 absorption as a function of frequency (or wavelength) around the spectral lines is shown in figure 7.4. The NESLAB cooler greatly reduces these thermal fluctuations. The signal from the pyrodetector is amplified using an ORIEL amplifier/readout model 70701, input to a lock-in amplifier. The reference signal for the lock-in amplifier is supplied by a digital signal generator connected to the laser control modulator, as shown in figure 7.3.

7.2. Experimental procedure

7.2.1. Calibration procedure

Calibration measurements were made to determine the dependence of the light transmitted through the fibre on the pressure of SF_6. The CO_2 laser was adjusted and left for a couple of hours to stabilise. The output from the monochromator was used as a power monitor and its output recorded in order to determine when the laser was operating in a stable mode. The cylinder containing the optical fibre was attached to the glow chamber; the valve between

the glow and corona chambers was closed, and SF_6 was bled through a needle valve into the previously evacuated glow chamber. The chamber was filled slowly, while the fibre output signal, S_f, was recorded on a chart recorder. The signal from the monochromator for monitoring power was recorded on another chart recorder, S_p. Chamber pressure was measured with the VAISALA PTB200 A digital barometer described in chapter 4. The temperature of the chamber was measured with a temperature probe attached to the wall of the chamber. Pressures were normalised to 25 °C. Values of S_f/S_p were recorded as a function of pressure, with S_f/S_p equal to one for zero pressure. Data were obtained both when SF_6 was slowly admitted to the chamber and when it was slowly pumped out of the chamber. Measurements for different incident angles were made in order to check the validity of equation 5.7.

During these experiments it was important that no leakage of SF_6 occurred into the laboratory, as can happen from exhaust lines. If SF_6 is released into the laboratory, it can remain for a long time, since the heavy SF_6 molecules replace the air at ground level. This "atmosphere" of SF_6 absorbs CO_2 laser light and even a small number of randomly moving SF_6 molecules in the path of the laser beam can cause fluctuations in the final detector signal. The effect was observed in the present work, before careful sealing of the exhaust line was completed.

7.2.2. SF_6 monitoring

A typical corona - monitoring experiment took nine days. The initial pressure of SF_6 was set at 90 kPa and the distance between electrodes (point and plane) at 10 mm. The current was maintained between 85 μA and 102 μA at a voltage of 35 kV. The current was recorded on a chart recorder. The total amount of charge transported during the nine-day discharge period was 63 Coulombs.

During this long time period the room temperature fluctuates and so the laser wavelength varies around the lasing line. This can lead to substantial errors as SF_6 absorption varies significantly over a frequency range of a few megahertz (figure 7.4). From observation

of the chart recorder it is clear when the laser is unstable: large fluctuations in power occur. Measurements obtained during laser instability were not used for data analysis.

The partial pressure of SF_6 during the discharge was calculated in the following manner. An interpolation formula was first established to fit a calibration plot of absorbance as a function of SF_6 pressure (section 7.4.1). This formula has the form

$$pressure_{SF_6}(kPa) = A + B\ln(signal) + C\ln^2(signal) \tag{7.4}$$

where $signal$ is the normalised signal obtained from the fibre output and the coefficients A, B and C are calculated for the pressure range between 50 kPa and 90.1248 kPa. This range was chosen because the partial pressure of SF_6 during the discharge fell from 90 kPa to around 70 kPa. Equation 7.4 with these coefficients was then used to calculate the partial pressure of SF_6 during the discharge from the measurements of fibre output.

The pressure and temperature in the chamber were monitored at all times during the experiment because the total pressure in the chamber continuously rises because of SF_6 dissociation. The pressure and temperature values were used to calculate the concentrations (as ratios) of the SF_6 and discharge by-products in the chamber at 1 atm and 25 °C. The partial pressure of the by-products is determined by subtracting the normalised partial pressure of SF_6 from the normalised total pressure.

7.3. Experimental results

7.3.1. Calibration

Before using this method to monitor the amount of SF_6 in a corona discharge the calibration was carried out. The calibration was performed as described in section 7.3.1.

Data for two incident angles θ (14° and 29°) were obtained for the transmitted signal T as a function of SF_6 pressure7.6. The absorbance $-ln[T(L,\lambda)]$ was plotted as a

function of pressure (figure 7.6.) and the curves are in agreement with the data obtained using a laser diode source (Messica *et al.*, 1994), which is shown in figure 5.4.

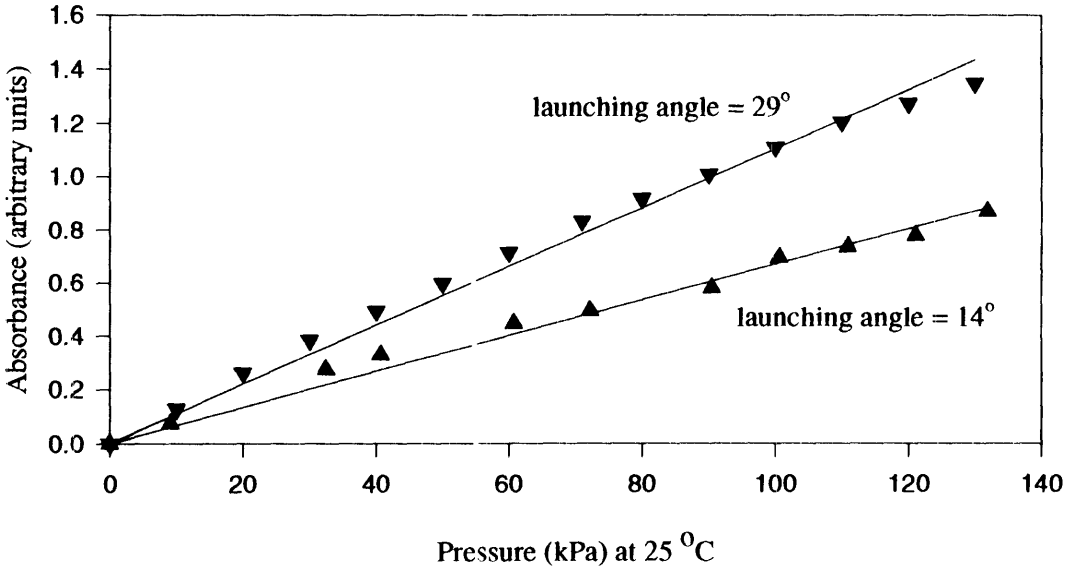

Figure 7.6. Calibration curves: evanescent-wave absorbance of CO_2 laser P(16) line versus pressure of SF_6 at 25 °C for silver halide optical fibre, at launching angles of 29° and 14°, with the lines of the best linear fit.

After these measurements were completed the incident angle was set to 45° in order to increase sensitivity further. For this setting it was necessary to slightly bend the fibre. Unfortunately, this introduced a nonlinearity into the absorbance curve (figure 7.7). The mechanical characteristics of a silver halide optical fibre are somewhat similar to those of copper wire. The fibre is soft and has low elasticity, so that attempts to straighten the fibre were unsuccessful. As a result, the measurements for 16° and 30° incident angles are also non-linear. The three curves are shown in figure 7.7.

The bend introduces higher order modes. The effect is similar to that of launching two laser beams into the fibre at different angles. In that case the absorption coefficient becomes (see equation 5.7)

$$\gamma_N = L\alpha\left(\Theta_1^2 + \delta_1^2\right) + L\alpha\left(\Theta_2^2 + \delta_2^2\right) \tag{7.5}$$

The effect can be observed in figure 7.7, for the 45° curve, where it appears that the bend creates more than one additional mode.

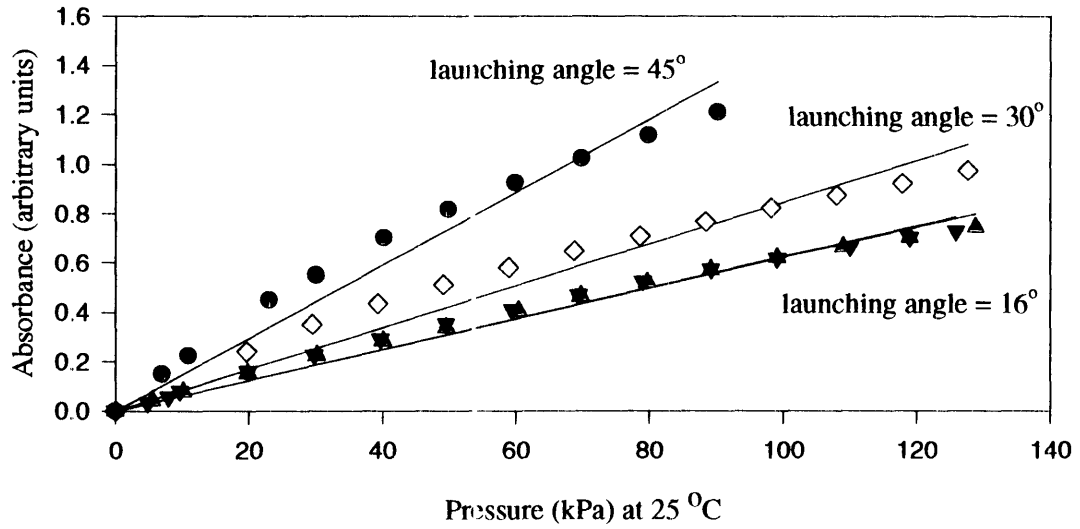

Figure 7.7. Calibration curves: evanescent-wave absorbance of CO_2 laser P(16) line versus pressure of SF_6 at 25 °C for silver halide optical fibre, at launching angles of 45°, 30° and 16°, with the lines of the best linear fit. The red and green triangles were recorded at the same incident angle. The red correspond to gas filling the chamber, and the green to the gas being pumped out of the chamber.

From both figures 7.6. and 7.7 it can be seen that the highest sensitivity was reached when the CO_2 laser beam was coupled to the fibre with an incident angle of 45°. This is in agreement with theory and equation 5.7. Further increase in the incident angle increases the sensitivity, but because of mechanical constraints it was not possible to go above 45°.

7.4.2. SF_6 in the corona discharge

Following the procedure described in section 7.3.2 the partial pressure and concentration of SF_6 was measured during the corona discharge and the results are presented in figure 7.8. As expected, there is a steady fall in the concentration of SF_6 molecules during a corona discharge.

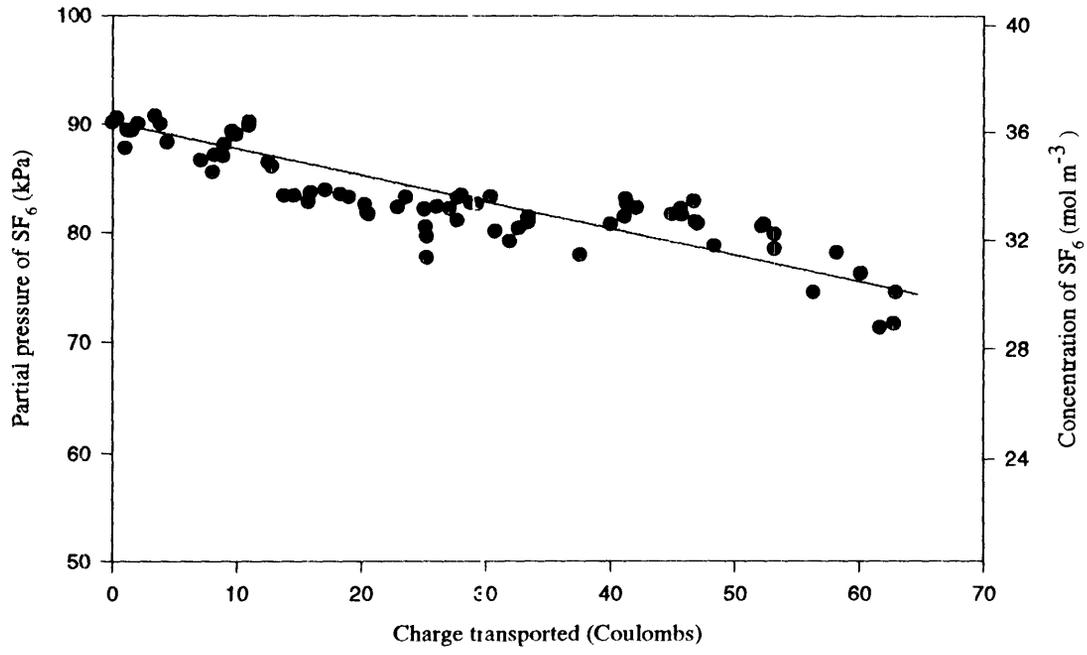

Figure 7.8. The amount of SF_6 during a corona discharge. The solid line is the best linear fit. The corona current was between 85 μA and 102 μA. The distance between point-plane electrodes was 10 mm. The applied voltage was around 35 kV. The initial pressure of SF_6 was 90.1248 kPa at 25 °C.

Because SF_6 dissociation results in production of by-products, the concentration of by-products builds up during the corona discharge. Figure 7.9 shows the increase in by-products concentration as a function of charge transport: for comparison, the SF_6 concentration is displayed. These results are in a good agreement with measurements made by Mortensen *et al.* (1994) using mass spectrographic analysis, and these are shown in figure 7.10.

The plot in figure 7.11 shows the concentration of SF_6 as a function of the input energy. This energy was obtained as a product of current and voltage between the electrodes. This energy is the sum of the heat that raises the temperatures of the gas and the electrodes, and the energy dissipated in chemical reactions, dissociation and radiation.

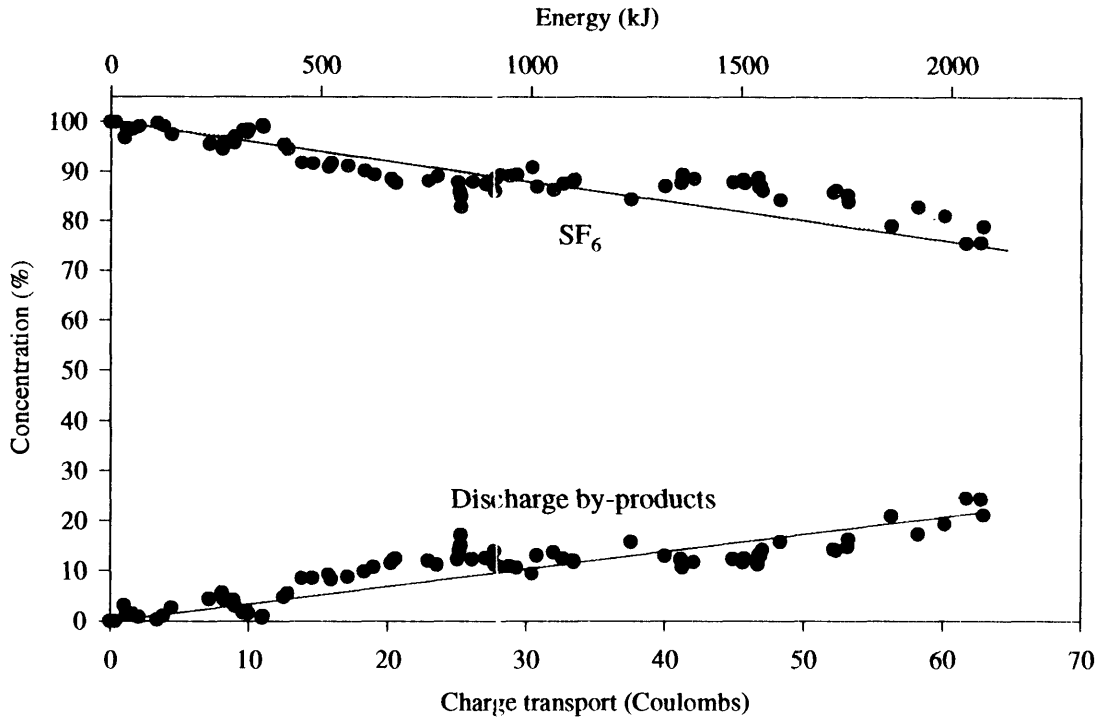

Figure 7.9. Concentration of SF_6 and discharge by-products in a corona chamber. The solid lines are the best linear fits. Same corona conditions as figure 7.8.

7.5. Discussion and conclusion

This work shows that an FEFA sensor can be used to monitor the degradation of SF_6 in a discharge. The fluctuations of the experimental points in figures 7.8 and 7.9 are probably due mainly to variations in the equilibrium of the laser. The experimental data on each of figures 7.8, 7.9 and 7.10 depict an overall linear trend and lines of best fit have been drawn to illustrate this. On the other hand, a plateau region on each curve may possibly exist in the range 20 C to 40 C. The fact that this trend is observed in both the present work and that of Mortensen *et al.* may be a coincidence but it is something that warrants further study. It should be possible to reduce laser fluctuations using a more stable CO_2 laser, and this might

help determine whether or not a plateau region does in fact exist. Furthermore, it may be that a lower power laser is more appropriate for these long-term measurements, since the output power of such lasers is easier to control and the power dissipation is lower.

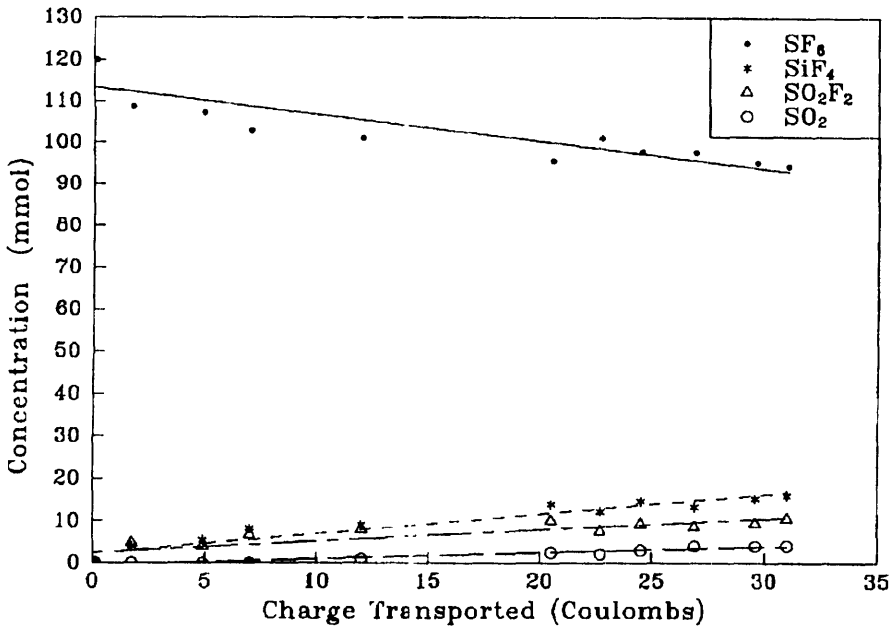

Figure 7.10. Concentration curves in a corona discharge obtained by using a mass spectrometer. Initial pressure of SF_6 is 100 kPa and the average discharge current is 75 μA (Mortensen *et al.*, 1994).

As mentioned in section 5.3.2, there is a significant ageing effect of silver halide optical fibres which can be compensated for by using a reference fibre. Another option is to replace the silver halide optical fibre with a different type of optical fibre that will transmit light of wavelength 10.6 μm, for example, a chalcogenide optical fibre. Recently there has been a significant improvement in the manufacturing of chalcogenide fibres (Busse *et al.*, 1996). The Naval Research Laboratory (NRL) has started production of sulphur-based ($As_{40}S_{60-x}Se_x$) fibres, for the 1 to 6 μm region and telluride-based ($Ge_aAS_bSe_cTe_d$) fibres for the 1 to 11 μm region. NRL has been able to reduce the transmission losses in chalcogenide fibres to an extent that the losses are now only slightly higher than those for silver halide optical

fibres. The chalcogenide fibres have the advantage of showing no ageing effect. Also, their durability is better.

Another disadvantage of the FEFA sensor for SF_6 monitoring is the high cost of CO_2 lasers. However, in an electrical plant containing several high-voltage insulating devices, sensing fibres could be placed in each, and the CO_2 laser radiation delivered from a single laser.

Since a CO_2 laser is much more powerful than a laser diode, pyrodetectors can be used rather than the more sensitive, but expensive, cryogenic antimonide or HgCdTe detectors.

The problem of wavelength drift can be solved in several different ways. For example, the small micrometer that is used to tune the resonant cavity length of the laser described in section 7.2.1 could be replaced with a piezocrystal that would vary the cavity length and lock onto the lasing line P(16). Otherwise the piezocrystal could be used to scan the frequencies around the lasing line, and measure the output signal from the fibre only when the laser goes through the maximum point corresponding to the lasing line P(16). Such a device was used in the experiments of Shimizu (1969).

Chapter 8

Summary and conclusions

In the electrical power industry, there is a need for a simple and reliable method of measuring the degradation of SF_6 in switchgear and other SF_6-filled high voltage devices. Such information can be useful for determining service-times for switchgear, and when the SF_6 should be replaced. At the moment there appears to be no sensor appropriate for such an application. Samples can be taken from the switchgear and analysed with laboratory instruments such as FTIR, but this is not cost effective, particularly when examining power systems in remote areas.

In the present work three methods have been devised for monitoring SF_6 degradation, and each has the potential to be made simple and compact enough to be built into switchgear systems. The three methods involve measurements of SF_6 refractivity, sulphur deposition, and evanescent-field absorption of SF_6 at 10.6 μm.

The last two methods, based on optical fibre sensing, may be closer than the first one to implementation as a final product for field measurement. Both can be used in high voltage devices. A sensor based on sulphur deposition can be made extremely simple, in that it requires only a source such as a red laser diode, a length of PCS optical fibre with a declad section and a detector. In order to avoid interference from the high voltage device, the source and detector can be placed remote from the device and the light can be delivered to and from it with optical fibres. This sensor is irreversible but this should not be a problem, since it needs to be replaced only when the SF_6 is replaced, and at that time maintenance involving dismantling of the device is likely to take place. The interferometer described in chapter 4 for refractivity measurement is neither simple nor compact and is not appropriate for field monitoring. However, the data obtained with the interferometer have shown that refractivity

measurement of the gas inside a high voltage device can provide useful information about the insulating condition of SF_6.

SF_6 monitoring is important in other devices that use SF_6 insulation. For example, when the amount of SF_6 by-products reaches 0.1 ppm in the ANU 14UD accelerator at the Australian National University in Canberra, ACT, the SF_6 has to be purified (Ophel *et al.*, 1983). The sampling method used for measuring this concentration of by-products is not practical for switchgear because a few litres of SF_6 are released during each measurement. According to Ophel the concentration of by-products in a circuit breaker should be detected with at least 100 ppm accuracy. This value is likely to vary for different switchgear systems: circuit breakers are known to operate efficiently with contaminant levels up to 0.2%, such as the one shown in figure 2.2 (Yamauchi *et al.*, 1985).

The sulphur deposition method is the most sensitive of the three techniques. The experiment described in chapter 6 was carried out at a pressure of 0.96 Torr of SF_6, and changes in deposition were readily detected. Indeed, in a high pressure device the deposition sensor could be too sensitive, with saturation occurring soon after the first fall in optical transmission (figure 6.11). However, the distribution of sulphur through the system is not uniform, and by choosing the right position in the chamber or by placing a shield around the fibre it should be possible to tune the sensor for appropriate SF_6 pressure and sensitivity.

The sensor based on evanescent-field absorption by SF_6 at 10.6 μm is less sensitive than the refractivity sensor. From the 45° calibration curve of figure 7.7 it can be seen that the SF_6 absorption sensor detects SF_6 pressure changes down to 0.67 kPa (~5 Torr), at filling pressures of around 100 kPa, this limit being set by the sensitivity of the lock-in amplifier. Increasing the incident angle of the CO_2 laser light into the fibre can increase the sensitivity further. Increasing the length of the fibre and choosing a more sensitive detector, such as an indium antimonide or HgCdTe photoconductive detector operating at 77 K, increases the sensitivity. In the long-term measurements on the corona discharge, the expected sensitivity of 0.67 kPa was not achieved because the CO_2 laser did not remain stable over long periods of time. With a more appropriate laser or laser diode it would be possible to achieve the expected value of sensitivity.

The refractive index measurement can detect changes of SF_6 concentration equal to 623 Pa (partial pressure at 25 °C) when the initial pressure of SF_6 is 1 atm. For a pressure of 10 atm (8 atm is the usual pressure in a single-pressure circuit breaker) this value is 658 Pa, which makes the precision of this method equal to 6.5×10^{-4}. This value is estimated using equations 4.4 and 4.21 and assuming that the only product of the discharge is SOF_2. The precision of the measurement of refractive index described in chapter 4 is 5×10^{-7}. The precision of the interferometer itself is higher than the precision of the pressure and temperature measurements, and so the overall precision of the method is limited by the accuracy of the pressure and temperature measurements. Temperature was measured with 0.1 °C accuracy and pressure with 0.02% (20 Pa) accuracy. The precision of the method would be significantly improved if the precision of temperature measurement were 0.01 °C and the precision of pressure measurement, 0.001%. Instruments with this precision are available but the cost is high, over US$5000 each. Even with this accuracy they are less accurate than the interferometer.

A practical field sensor does not need the high precision of the Lee-Woolsey polarisation interferometer used in this work. Bulk-optic devices using white light or low-coherence radiation can be designed to be small. They do not require initialisation at each measurement, so that measurements can be made continuously. There are many different types of low-coherence interferometers, including those using a multimode laser diode as source (Wang *et al.*, 1995B); an arc lamp (Sáinz C. *et al.*, 1994); a laser diode that works just below threshold (Wang *et al.*, 1995A); 2 lasers (Wang *et al.*, 1995B); a white light source and interference filters (Ludman *et al.*, 1995); an LED source (Wang *et al.*, 1995A); with PDA (linear photodetector array) detector (Schnell *et al.*, 1996); a CCD (charge coupled device) array; and a single photodiode with electronics and positioner for fringe locking (Ludman *et al.*, 1995). The accuracy of 1 part in 10^6 achieved by the latter is sufficient for detecting changes in the refractive index of the gas mixture inside the SF_6-filled device. However, pressure and temperature also must be measured so that the refractive index at 1 atm and 25 °C can be obtained.

In a circuit breaker changes in refractive index are larger than those experienced in the present work, because of the higher pressures used in the former. This means that a refractometer based on surface plasmon resonance could be considered as a simple solution (Jorgenson and Yee, 1994). Its sensitivity of 5×10^{-5} may be enough for monitoring high pressure systems. For low pressures, a bulk-optic device based on surface plasma resonance has a resolution of 4×10^{-6} (Kunz *et al.*, 1996). One of these refractometers together with a precise pressure meter and thermometer would be able to reach the sensitivity of 10^{-4} required for circuit-breaker monitoring. The arrangement chosen needs to be resistant to the high electric and magnetic fields and the electromagnetic radiation that exist in switchgear under usual working conditions.

Evanescent-field absorption at 10.6 μm is a direct method and it does give information about the remaining SF_6, which is the information required. The refractive index measurement and sulphur deposition methods require separate calibration for each high-voltage device and if there is some defect in the device, such as a high level of water vapour in the fill of SF_6, a wrong measurement can result. Because of this, precautions must be taken and sensors for other parameters may have to be included. The SF_6 absorption sensor is almost immune to such problems, because it provides information about the SF_6 wherever it is placed. However, at the moment it would be the most expensive option, mainly due to the high cost of the 10.6 μm radiation source. Furthermore, a CO_2 laser is bulky, a lead salt infrared laser diode requires a cryogenic cooler, and the life time of a high power tungsten filament halogen light bulb or Nernst glower is short. The cost of a lead salt laser diode for 10.6 μm is around US$4000, but it needs a cryogenic cooler which costs a further US$15 000. Liquid nitrogen can be used to cool some of these diodes. Another solution could be an infrared light-emitting diode, operating at room temperature. Work on mid-infrared LEDs at room temperatures is still in the experimental stage and the maximum peak output power achieved so far is 10 μW (Tang *et al.*, 1995B). These are currently under development in a few laboratories.

The work presented here has demonstrated the feasibility of the three optical sensors. The sulphur deposition method has enough sensitivity to be employed for SF_6

monitoring in switchgear, while the other two are close to the targeted sensitivity of 10^{-4}, but more work is needed to produce a practical sensor. Indeed, more work is required to improve all three techniques.